Biophysical Characterization of Recombinant Human Bcl-2 and Its Interactions with an Inhibitory Ligand, Antimycin A[†]

Kristine M. Kim,[‡,▽] Chris D. Giedt,[§] Gorka Basañez,[∥] Jason W. O'Neill,[‡] John J. Hill,[⊥] Yi-Hong Han,[‡] Shie-Pon Tzung,[§] Joshua Zimmerberg,[∥] David M. Hockenbery,[§] and Kam Y. J. Zhang*[,‡]

Divisions of Basic Sciences and Clinical Research, Fred Hutchinson Cancer Research Center, 1100 Fairview Avenue North, Seattle, Washington 98109, Laboratory of Cellular and Molecular Biophysics, National Institute of Child Health and Human Disease, National Institutes of Health, Bethesda, Maryland 20892, and Department of Protein Biochemistry, ICOS Corporation, 22021 20th Avenue, Southeast, Bothell, Washington 98021

Received October 11, 2000; Revised Manuscript Received January 16, 2001

ABSTRACT: Apoptosis is an essential physiological process, regulated by the family of Bcl-2-related proteins. However, the molecular mechanism by which Bcl-2 regulates apoptosis still remains elusive. Here we report the functional studies of recombinant human Bcl-2 with the deletion of 22 residues at the C-terminal membrane-anchoring region (rhBcl-2Δ22). Characterization of rhBcl-2Δ22 showed that the recombinant protein is homogeneous and monodisperse in nondenaturing solutions, stable at room temperature in the presence of a metal chelator, and an α-helical protein with unfolding of secondary structure at a T_m of 62.8 °C. Optimal membrane pore formation by rhBcl-2Δ22 required negatively charged phospholipids. The existence of a hydrophobic groove in rhBcl-2Δ22 was demonstrated by the fluorescence enhancement of the hydrophobic ANS probe with which a pro-apoptotic Bak BH3 peptide competed. The respiratory inhibitor antimycin A also bound to the hydrophobic groove of rhBcl-2Δ22 with a K_d of 0.82 μM. The optimal binding conformation of antimycin A was predicted from molecular docking of antimycin A with the hBcl-2 model created by homology modeling. Antimycin A selectively induces apoptosis in cells overexpressing Bcl-2, suggesting that hydrophobic groove-binding compounds may act as selective apoptotic triggers in tumor cells.

Programmed cell death by apoptosis is an essential physiological process for the selective elimination of cells, including those involved in a variety of biological events such as development and host defense mechanisms (*1*). Dysregulated apoptosis contributes to the pathogenesis of tumors, autoimmunity, and degenerative diseases (*2*, *3*). In particular, enhanced expression of anti-apoptotic Bcl-2-related proteins in cancer cells has been implicated in resistance to currently available antineoplastic agents (*4*). Consequently, elucidation of biochemical mechanisms of apoptosis holds great promise for developing new strategies for prevention, detection, diagnosis, and treatment of those diseases, as demonstrated by the major interest in apoptosis research in the past decade.

The proteins of the Bcl-2 family play a pivotal role in the regulation of apoptosis. The members of this family can be divided into three subfamilies based on several conserved sequence motifs known as Bcl-2 homology (BH) domains. The anti-apoptotic members (Bcl-2, Bcl-x_L, Mcl-1, Bcl-w, A1, Boo, and Ced-9) share all four BH domains, designated as BH1−4; the pro-apoptotic members Bax, Bak, Bok, and Bcl-x_S contain BH1−3 domains, but other pro-apoptotic members (Bad, Bik, Bid, and Egl1) only have a BH3 domain in common with Bcl-2. The number of Bcl-2-related proteins has been significantly and continuously expanded since the discovery of Bcl-2, from representatives in mammalian organisms to *Drosophila melanogaster* (*5*). However, the molecular mechanism by which Bcl-2 proteins regulate apoptosis remains unclear.

Elucidation of how Bcl-2 proteins regulate apoptosis is complicated by multiple apparent functions, which involve protein−protein interactions as well as formation of pores in lipid membranes. The members of the Bcl-2 family can either homodimerize or heterodimerize with other members; for example, Bcl-2 forms heterodimers with Bax, Bcl-x_L, A1, and Bad (*6*). The BH1−3 domains of Bcl-x_L form a hydrophobic groove at its three-dimensional surface (*7*, *8*), which is the docking site for the BH3 domains of pro-apoptotic binding partners. The solution structure of Bax revealed the binding of the C-terminal hydrophobic tail to the hydrophobic groove formed by domains BH1−3, suggesting a regulatory mechanism for the simultaneous control over its mitochondrial targeting and dimer formation (*9*). The BH4 domain is not essential for the dimerization, but its deletion alters the function of Bcl-2 from anti-apoptotic to

[†] This work was supported by American Cancer Society Grant RPG-97-173-01-LBC (K.Y.J.Z.) and NIH Grant CA15704-26 (D.M.H.).

* To whom correspondence should be addressed. E-mail: kzhang@fhcrc.org. Phone: (206) 667-4220. Fax: (206) 667-3331.

[‡] Division of Basic Sciences, Fred Hutchinson Cancer Research Center.

[§] Division of Clinical Research, Fred Hutchinson Cancer Research Center.

[∥] National Institutes of Health.

[⊥] ICOS Corporation.

[▽] Present address: Immunex Corporation, 51 University Street, Seattle, WA 98101.

10.1021/bi002368e CCC: $20.00
Published on Web 03/29/2001

pro-apoptotic (*10*). Isolated peptide pro-apoptotic BH3 domains, and by implication the whole proteins, are inhibitors of the anti-apoptotic proteins and can induce apoptosis. Bcl-2 also interacts with unrelated proteins such as Raf-1 and calcineurin (*4*). These protein interactions appear to modulate the apoptotic function of Bcl-2 (*6*, *11*−*14*). Recently, Lee et al. (*15*) reported a new Bcl-2 binding protein, Bis, that enhances the anti-apoptotic function of Bcl-2, while possessing only weak anti-apoptotic activity by itself, further implicating Bcl-2 protein interactions in the regulation of apoptosis.

Bcl-2, Bcl-x_L, and Bax also form large conductance pores in synthetic lipid membranes (*16*−*18*). Membrane channel formation by Bcl-2 proteins is thought to be involved in the anti- and pro-apoptotic effects of these factors, but the critical species that are transported are unknown (*7*, *19*, *20*). Several studies have implicated altered membrane permeability in apoptosis. Bcl-2 and Bcl-x_L are targeted to the outer mitochondrial membrane by a C-terminal hydrophobic sequence that also functions as a membrane anchor. Changes in mitochondrial membrane potential, either early hyperpolarization or delayed depolarization, occur during apoptosis and are antagonized by Bcl-2 (*21*, *22*). Bcl-x_L has been shown to maintain ADP−ATP exchange across the inner mitochondrial membrane, presumably by affecting the permeability of the mitochondrial outer membrane (*23*). Finally, increased mitochondrial matrix pH (and decreased cytoplasmic pH) has been recently described as an early event in apoptosis and is also prevented by Bcl-2 (*24*). The precise role, if any, of Bcl-2 membrane pores in any of these alterations in transmembrane gradients during apoptosis has not been defined to date.

Structural and functional studies of Bcl-2 in complex with any binding partners should improve our understanding of how Bcl-2 regulates apoptosis. Unfortunately, such studies have been hampered by difficulties in obtaining sufficient quantities of Bcl-2 protein in a homogeneous state. Methods previously described for the purification of Bcl-2 result in very low yields (*25*), requiring a large-scale fermentation and/or purification from inclusion bodies (*26*, *27*) associated with prohibitive time and cost. Previously, we have shown that hBcl-2 with a deletion of the hydrophobic C-terminal tail (hBcl-2Δ22)[1] retains anti-apoptotic function (*28*). Accordingly, we cloned and expressed hBcl-2Δ22 in *Escherichia coli*. Here we describe a simple and rapid purification method for recombinant hBcl-2Δ22 from the soluble bacterial lysate, resulting in ∼9 mg of homogeneously folded, active protein suitable for functional and structural studies per liter of cell culture. Initial biophysical characterization of rhBcl-2Δ22 reveals a hydrophobic site which binds a pro-apoptotic BH3 domain peptide, consistent with the hydrophobic groove in a computational model of the hBcl-2 structure, and pH-dependent pore formation in negatively charged lipid membranes. We also demonstrate that an inhibitor of mitochondrial respiration, antimycin A, binds to the hydrophobic BH3 binding site in rhBcl-2Δ22.

[1] Abbreviations: AA, antimycin A; ADR, adriamycin; CL, cardiolipin; rhBcl-2Δ22, recombinant human Bcl-2 with deletion of 22 C-terminal residues; LUVs, large unilamellar vesicles; PC, phosphatidylcholine; PG, phosphatidylglycerol; PI, phosphatidylinositol; pI, isoelectric point; PS, phosphatidylserine; TM, transmembrane.

MATERIALS AND METHODS

Cloning of hBcl-2Δ22. Human Bcl-2Δ22 was obtained by PCR using a forward primer with the sequence TTTATAACATATGGCGCACGCTGGGAGAACGG and a reverse primer with the sequence GATTTACTCGAGCAGAGACAGCCAGGAGAA. The PCR product, hBcl2Δ22, was digested with *Nde*I and *Xho*I and ligated into *Nde*I−*Xho*I-restricted pET22b(+) (Novagen). *E. coli* strain DH5α cells were transformed with pET22b-hBcl2Δ22 under ampicillin and kanamycin selection. DNA sequencing by dideoxy chain termination confirmed the correct nucleotide sequence.

Expression and Purification of rhBcl-2Δ22. A single colony of *E. coli* BL21 (DE3) cells harboring pUBS520 encoding human argU tRNA and pET22b-hBcl2Δ22 was used to inoculate 2× YT medium containing 200 mg/L ampicillin and 50 mg/L kanamycin. Cells were grown to an OD_{600} of 0.6 at 37 °C, and the expression of protein was induced with 0.1 mM isopropyl β-D-thiogalactoside at 30 °C. The cells were harvested by centrifugation, resuspended in 1:5 (w/v) PEB [50 mM Tris (pH 8.5), 0.2 M NaCl, 0.2 mM PMSF, 5 mM βME, 5 mM imidazole, and 1% (v/v) glycerol], and stirred for 20 min at 4 °C. Lysozyme (0.2 mg/mL) and a pinch of DNaseI were added to the cell mixture, and the solution was stirred for an additional 20 min. Cells were disrupted by pulse sonication at 70% output, and the cell debris was removed by centrifugation (30 min at 31000*g*) at 4 °C. The soluble fraction was loaded onto a Ni−NTA column (Qiagen) equilibrated with PEB, and unbound proteins were removed with PEB containing 40 mM imidazole. Proteins were eluted from the column with PEB containing 200 mM imidazole, pooled, and dialyzed against buffer containing 50 mM Tris (pH 8.5), 200 mM NaCl, 1 mM DTT, 2 mM EDTA, and 0.2 mM PMSF at 4 °C overnight. The dialyzed protein was concentrated to about 10 mg/mL and fractionated on Superdex 75 gel filtration column (Pharmacia Biotech Inc.) equilibrated in dialysis buffer. The peak containing rhBcl-2Δ22 was pooled, exchanged to low-salt buffer, and loaded onto an anion exchange column (MonoQ, Pharmacia Biotech Inc.) to separate an acidic contaminant protein. The protein yield at each purification step was determined by the Bradford assay; the concentration of the purified rhBcl-2Δ22 at the end of purification was determined using an ϵ_{280} of 43 430 M^{-1} cm^{-1} obtained by the method of Mach et al. (*29*).

Electrophoresis and Western Blotting. SDS−PAGE was performed as described by Laemmli (*30*) on 15% acrylamide followed by either silver or Coomassie blue R-250 staining. Isoelectric focusing (IEF) was performed on a Pharmacia Ampholite PAGplate gel (pH 3−9) using a Pharmacia PHAST system, and gels were silver stained. Prestained isoelectric markers (Bio-Rad) were run on the same gel (600 V, 5 mA, 3.5 W, 1.5 h). For Western blotting, proteins were separated by 15% SDS−PAGE and electroblotted onto a nitrocellulose membrane. Immunodetection of rhBcl-2Δ22 was accomplished using hamster anti-Bcl-2 monoclonal antibody (1:100) followed by a biotinylated goat anti-hamster antibody (1:1000) (Vector, Burlingame, CA) and HRP-conjugated streptavidin (1:5000) (Zymed, South San Francisco, CA). Chemiluminscence (ECL, Amersham, Arlington Heights, IL) was used for detection.

Mass Spectrometry. Mass measurements were performed with a Finnigan LCQ quadrupole ion trap mass spectrometer (Finnigan-MAT, San Jose, CA) and by matrix-assisted laser desorption/ionization (MALDI) mass spectrometry (Biopercceptive, Farmington, MA). The matrix used for MALDI-TOF was recrystallized α-cyano-4-hydroxycinnamic acid (Sigma). The sample was added to a saturated solution of a 2:1 aqueous 0.1% trifluoroacetic acid/acetonitrile matrix. One microliter of the solution was placed on the probe of the mass spectrometer and allowed to dry before analysis.

Dynamic Light Scattering (DLS). Hydrodynamic properties were measured using a DynaPro molecular sizing instrument (Protein Solutions, Ltd.) equipped with a temperature controller. All samples were filtered through a 0.1 μm membrane before analysis. Lysozyme (20 mg/mL) in 40 mM sodium acetate (pH 5.5), 0.5% (v/v) NaCl, and BSA in PBS (2 mg/mL; Pierce) were used as controls. Various concentrations of rhBcl-2Δ22 were used to measure hydrodynamic parameters following the manufacturer's instructions.

Spectroscopy. Far-UV circular dichroism (CD) spectra were obtained with samples in 10 mM phosphate buffer (pH 8) using an AVIV 62A DS spectropolarimeter equipped with a thermoelectric cell and calibrated with a (+)-10-camphorsulfonic acid standard (Sigma). Spectra were recorded using a 1 mm cell path length in wavelength increments of 0.2 nm. The presented spectrum is the average of three scans of protein corrected for background solvent effects by subtraction of the buffer blank. Data are presented as the molar ellipticity per residue, $[\Theta]_{MRW}$, in degrees per square centimeter per decimole using the relation $[\Theta]^{\lambda}_{MRW} = (\Theta^{\lambda}_{obs}\text{-}MW_r)/(cdN_A)$, where Θ^{λ}_{obs} is the measured ellipticity in millidegrees by the instrument at wavelength λ, MW_r is the molecular weight of rhBcl-2Δ22, c is the protein concentration in milligrams per milliliter, d is the path length in centimeters, and N_A is the number of amino acids in rhBcl-2Δ22. Thermal unfolding of rhBcl-2Δ22 was followed by measuring the change in ellipticity at 222 nm as a function of temperature. The temperature was changed at the rate of 0.5 °C/min in the range of 25−82.5 °C, and the sample was equilibrated for 0.5 min before each measurement was made every 2.5 °C with a response time of 30 s.

Liposome Studies. Phosphatidylcholine (PC), phosphatidylglycerol (PG), phosphatidylserine (PS), cardiolipin (CL), and phosphatidylinositol (PI) from natural sources were obtained from Avanti Polar Lipids (Alabaster, AL). Large unilamellar vesicles (LUVs) were formed by extrusion according to the method of Mayer et al. (*31*). Dry films of lipid were rehydrated in aqueous solutions containing either 12.5 mM ANTS, 45 mM DPX, and 10 mM Hepes or 60 mM calcein and 10 mM Hepes (pH 7.0), subjected to 5−10 freeze−thaw cycles, and extruded 10 times through two polycarbonate filters with a 0.1 μm pore size (Nucleopore, Pleasanton, CA). Nonencapsulated material was removed using a Sephadex G-10 column loaded with 100 mM KCl and 10 mM Hepes (pH 7.0). The size of the final liposome preparation was routinely checked by a Coulter N4 Plus Particle-Sizer and was close to the expected value (~100 nm). Lipid concentrations were measured by the ammonium ferrothiocyanate method (*32*). Fluorescent measurements were performed at 37 °C in a 1 cm path length cuvette using an SLM-2 Aminco-Bowman luminescence spectrometer (Spectronic Instruments, Rochester, NY). Release of fluorescent markers was quantified on a percentage basis according to the equation

$$\% \text{ release} = (F_f - F_0/F_{100} - F_0) \times 100$$

F_f being the measured fluorescence after protein addition, F_0 the initial fluorescence of the intact LUV suspension, and F_{100} the fluorescence after complete disruption of vesicle integrity by addition of Triton X-100 (final concentration, 0.2% w/v). For ANTS, the excitation and emission wavelengths were 355 and 520 nm, respectively (8 nm slit width). For calcein, the excitation and emission wavelengths were 490 and 520 nm, respectively (2 nm slit width). Final extents of leakage were obtained after the fluorescence intensity reached a plateau. The maximum level of release of entrapped dyes was determined by Triton X-100 addition (final concentration, 0.6 mM). Unless otherwise stated, protein and lipid concentrations were 100 nM and 60 μM, respectively.

Transfection. Both Bcl-2 and full-length Bcl-x_L were cloned into the mammalian expression vector pSFFV (*33*). Mouse hepatocyte TAMH cells were transfected by lipofection (Lipofectamine, Life Technologies, Rockville, MD) with pSFFV (control), pSFFV-Bcl-2, and pSFFV-Bcl-x_L plasmids. Transfectants were selected for the acquisition of neomycin resistance in 750 μg/mL G418. Bulk transfectants were cloned by limiting dilution, and individual clones were screened by immunoblot to determine the level of protein expression.

Cell Viability following ANS, Antimycin A, and 2-Methoxyantimycin A Treatment. Equal numbers of stably transfected cells were plated on 12-well tissue culture plates. Experiments were performed when cells reached approximately 70−80% confluence. Antimycin A, ANS (both from Sigma, St. Louis, MO), and 2-methoxyantimycin A (*34*) were dissolved in DMSO and used to treat cells at the indicated concentrations. Control cultures were treated with vehicle alone. Six hours after treatment, cells were trypsinized and cell viability was determined by trypan blue dye exclusion. The number of viable cells was counted, expressed as a fraction of total cells counted (100−200 per well), and normalized to the control group, i.e., % cell viability = (viable cells in treated group/viable cells in control group) × 100%.

Fluorescence Spectroscopic Measurements. Fluorescence spectroscopic studies were performed on a Hitachi F-2500 fluorescence spectrophotometer equipped with a thermostatic cell holder. All measurements, unless otherwise indicated, were conducted as described below. The excitation wavelengths for ANS (Sigma) were 374 nm, and emission was recorded from 400 to 600 nm. Samples were prepared in 50 mM Tris-HCl buffer [0.2 M NaCl, 2 mM EDTA, and 0.5% (v/v) glycerol (pH 8.0)] and checked for the "inner filter effect" over the range of ANS and antimycin A concentrations used for this study. Blanks containing an equal concentration of flurophore as the samples were used as a control in all measurements, and the necessary corrections were made. The concentrations of ANS solution were quantitated using an extinction coefficient of $6.8 \times 10^3\ M^{-1}\ cm^{-1}$ at 370 nm. The optimal stoichiometric ratio for ANS interaction with rhBcl-2Δ22 was determined by the method of continuous variation [Job plot (*35*)]. Job plot was

constructed using the enhanced fluorescence of ANS when ANS binds to rhBcl-2Δ22, while keeping the total concentration of ANS plus rhBcl-2Δ22 at 30 μM. For displacement experiments, ANS was mixed with rhBcl-2Δ22 and the mixture allowed to reach equilibrium at 4 °C. The various concentrations of BH3 peptide corresponding to the BH3 domain of Bak (72-GQVGRQLAIIGDDINR-87; Colorado State University) were added to the mixture, and the change in the fluorescence of ANS was measured. Measurements of the fluorescence spectra of antimycin A were carried out as for ANS, except for the following changes. The wavelengths for excitation and maximal emission for antimycin A (Sigma) were 335 and 428 nm, respectively, at 15 °C. The concentration of antimycin A was determined using an extinction coefficient of 7.24 mM^{-1} cm^{-1} at 320 nm.

Measurement of Binding Affinities for Bcl-2. Isothermal titration calorimetry (ITC) experiments aimed at assessing the binding of antimycin A_3 and BH3 peptide to rhBcl-2Δ22 were conducted at 25 °C, using a VP-ITC microcalorimeter (Microcal, Inc., Northhampton, MA) following the standard instrumental procedures. The 1.3 mL sample cell was filled with buffer containing rhBcl-2Δ22 (2−13 μM). The syringe was filled with a ligand solution of antimycin A_3 (40 μM) or BH3 peptide (180 μM). The binding experiments were carried out with 25 × 10 μL injections of ligand solution at 3.5−4 min intervals with continuous stirring at 200 rpm. Control experiments were performed to measure the heats of ligand dilution into buffer, which were subtracted from the reaction data prior to fitting. Heats of protein dilution, by buffer, were corrected for either by setting the upper plateau of the binding curve to 0 kcal/mol or from control experiment without ligand addition. The integrated heat effects were analyzed by nonlinear regression methods (*36*) using a standard ORIGIN software package supplied by Microcal. The experimental data fit well to a model for simple binding to a single class of sites, yielding estimates of the apparent number of binding sites (N) on the protein, the association binding constant [K (inverse molar)] and the enthalpy of binding [ΔH (kilocalories per mole)]. The entropies [ΔS (calories per kelvin per mole)] associated with the binding reactions were calculated from the standard expression:

$$\Delta G^\circ = -RT \ln K = \Delta H^\circ - T\Delta S^\circ$$

rhBcl-2Δ22 protein solutions were dialyzed extensively into 10 mM Na_2HPO_4/NaH_2PO_4 (pH 7.0) buffer followed by addition of acetonitrile to 5% (v/v) for antimycin titrations, or into 10 mM Na_2HPO_4/KH_2PO_4, 137 mM NaCl, 2.7 mM KCl buffer (pH 7.0) for BH3 peptide titrations. The low-salt, acetonitrile buffer was required to maintain solubility of antimycin A for the antimycin titrations because of its low solubility, whereas the higher ionic strength in the BH3 peptide buffer was necessary to decrease the level of nonspecific binding. Protein concentrations were determined from UV absorbance measurements at 280 nm, using an ϵ_{280} of 43 430 M^{-1} cm^{-1} estimated by the method of Mach et al. (*29*). Antimycin samples were prepared from a 25 mM stock solution in 100% acetonitrile, diluted 20-fold into dialysis buffer, and shaken for 2 h to reach a maximum solubility of ~40 μM. Antimycin concentrations were quantified, using a standard curve, by HPLC analysis. BH3 peptide was prepared by addition of PBS dialysis buffer to peptide powder that was weighed with an accuracy of ±1 μg.

Caspase-3 Activation Assay. Mouse hepatocyte TAMH cells that were transfected with pSFFV-Bcl-2 plasmids were treated with 2 μg/mL antimycin A and lysed at the indicated time points in hypotonic lysis buffer [25 mM HEPES (pH 7.5), 5 mM $MgCl_2$, 5 mM EDTA, 5 mM DTT, 2 mM PMSF, 10 μg/mL pepstatin A, and 10 μg/mL leupeptin]. Cell lysates (75 μg/mL protein) were incubated with 50 μM fluorogenic caspase-3 substrate (Ac-DEVD-AMC, Promega) in assay buffer [100 mM HEPES (pH 7.5), 10% sucrose, 0.1% CHAPS, and 10 mM DTT] at 30 °C for 30 min. Fluorescence was measured at an excitation wavelength of 360 nm and an emission wavelength of 460 nm.

Molecular Modeling. The molecular model of human Bcl-2 was generated by a computational modeling method using the crystal structure of human Bcl-x_L (*7*) as a template. Both Bcl-2 and Bcl-x_L share the four conserved regions, BH1−4, found in the Bcl-2 family as well as the membrane-anchoring tail at the C-terminus. Overall, the sequences of Bcl-2 and Bcl-x_L are 43% identical. Their level of sequence identity reaches 62% when the flexible loop region between the BH4 and BH3 regions is excluded. The high degree of sequence similarity suggests that they adopt the same overall structural fold. The sequences of Bcl-2 and Bcl-x_L were aligned with CLUSTAL-W (*37*). This alignment provided a means of anchoring the residues in Bcl-2 to the corresponding positions in the Bcl-x_L structure. The program MODELLER (*38*) was used to search for the optimal side chain packing in the Bcl-2 structural model and to refine the main chain positions as well using the simulated annealing molecular dynamics protocol. The ideal bond lengths and angles were used as a restraint during the simulated annealing optimization process. To avoid being trapped in the local minimum of the global energy landscape, 50 independent runs of optimization starting from a random seed were carried out to generate 50 models of Bcl-2. All these models were analyzed by three independent structure validation programs, PROCHECK (*39*), VERIFY_3D (*40*), and ERRAT (*41*), which evaluates the distribution of main chain dihedral angles and deviation of bond lengths and angles from ideal, the side chain environment in the model, and the distribution of nonbonded atoms in the neighborhood of an atom, respectively. These analyses confirmed the model with the lowest energy as calculated by MODELLER is the most consistent with the evaluation criteria used in the three structure validation programs. This model with the lowest energy was thus chosen as the final model for the human Bcl-2 structure.

Docking. The potential binding site for antimycin A_3 on human Bcl-2 was determined by a molecular docking algorithm. The Bcl-2 model used in the docking was created by the MODELLER program. The antimycin A_3 model was generated from the crystal structure of antimycin A_1 (*42*) through the deletion of two methyl groups. If one starts from the Bcl-2 model, a molecular docking program suite, DOCK (*43*), was used to systematically move antimycin A_3 along the molecular surface of Bcl-2 and search for potential binding sites. The binding energy for each conformation of antimycin A_3 was evaluated, and those conformations with the lowest energy were saved and analyzed.

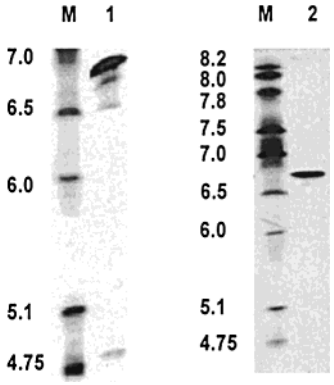

FIGURE 1: Isoelectric focusing electrophoresis of rhBcl-2Δ22 after Superdex 75 chromatography (lane 1) and at the end of the final purification step (lane 2). Lanes labeled M contained the isoelectric markers.

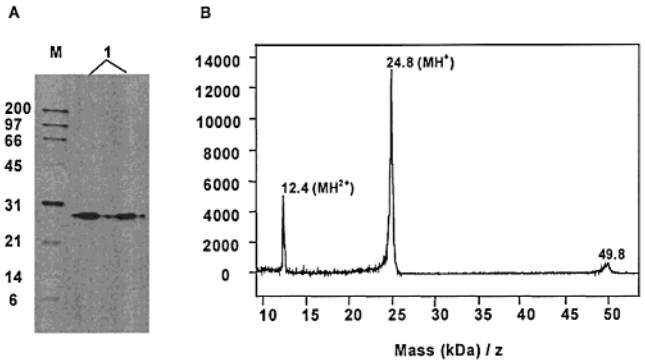

FIGURE 2: Identification of recombinant protein as hBcl-2Δ22. (A) Analysis by Western blotting with anti-Bcl-2. Lanes M and 1 contained biotinylated markers (kilodaltons) and a protein sample pooled from Superdex 75 chromatography and a positive control, respectively. (B) Analysis by the MALDI-TOF mass spectrometer of purified rhBcl-2Δ22.

RESULTS

Expression and Purification of rhBcl-2Δ22. We expressed rhBcl-2Δ22 with a His_6 tag at the C-terminus to facilitate purification by affinity chromatography. Induced rhBcl-2Δ22 expression in *E. coli* cells harboring pUBS520 encoding human argU tRNA that recognize the rare Arg codons for *E. coli* (*44*, *45*) represented more than 15% of total cellular protein. Approximately 5% of Bcl-2 appeared in the soluble lysate fraction. However, the level of protein expression was significantly reduced when *E. coli* lacking pUBS520 was used as a host (our unpublished result). A high rhBcl-2Δ22 expression level probably results from reduced codon bias for Arg. Subsequent purification and characterization of rhBcl-2Δ22 started with the protein expressed in the soluble fraction to avoid the time, cost, and relatively low yields often associated with protein refolding of insoluble inclusion bodies. Single-step Ni−NTA affinity chromatography resulted in about 90% pure protein. Subsequent size exclusion chromatography showed rhBcl-2Δ22 elutes as a monomer in solution, and the protein pooled from this step gave a single protein band when analyzed by SDS−PAGE (data not shown). However, analysis by IEF electrophoresis showed multiple protein bands, with a predominant band at an isoelectric point (pI) of 6.8, in excellent agreement with the calculated pI (6.89), and three other minor bands near pI 6.6, 6.5, and 4.8 (Figure 1, lane 1). Further purification by anion exchange chromatography resulted in a single protein band on IEF (Figure 1, lane 2). Purification of rhBcl2Δ22 gave a very high yield of electrophoretically homogeneous protein, typically ~9 mg/L of cell culture at the end of the final purification step (data not shown).

Analysis of rhBcl-2Δ22. Western blotting confirmed that the purified 25 kDa protein is hBcl-2 (Figure 2A). The MALDI-TOF mass spectrum exhibited a singly charged ion at 24.8 kDa/*z* and a doubly charged ion peak at 12.4 kDa/*z*, demonstrating the purity and homogeneity of rhBcl-2Δ22 (Figure 2B). The small minor ion peak at 49.8 kDa/*z* is the dimer of rhBcl-2Δ22. Analysis by electrospray mass spectrometry gave mass/*z* ion peaks corresponding to 24 974 ± 1 Da, which is in excellent agreement with the calculated average mass based on the amino acid sequence with the leader methionine removed (24 975 Da; data not shown). N-Terminal sequencing by sequential Edman degradation revealed the expected amino acid sequence, Ala-His-Ala-Gly-Arg, if the f-Met were removed by an endogenous methionine aminopeptidase.

Table 1: Dynamic Light Scattering Analysis of hBcl-2Δ22

			Bcl-2Δ22	
	lysozyme	BSA	without glycerol	with glycerol[a]
R_H[b]	1.8	3.54	2.6	2.92
polydispersity	<0.3	<0.4	1.05	0.67
BASE	1.000	1.003	1.001	1.000
SOS	<0.2	0.51	3.53	0.56

[a] The glycerol concentration was 0.5% (v/v). [b] Hydrodynamic radius.

Self-Association of rhBcl-2Δ22. We noticed during protein purification that the addition of glycerol in the purification buffer was necessary to prevent protein aggregation. In the absence of glycerol, proteins eluted from the size exclusion column at volumes corresponding to the aggregated protein as well as the expected monomeric 25 kDa peak (data not shown). The ratio of aggregated to monomeric peaks was significantly diminished in buffers containing glycerol (data not shown). The polydispersity or self-association of rhBcl-2Δ22 was also analyzed by dynamic light scattering (DLS). The polydispersity number from DLS represents the standard deviation of the size distribution based on the experimentally measured mean hydrodynamic radius, R_H. In the absence of glycerol, the polydispersity number in relation to R_H was 1.05, indicating self-association of rhBcl-2Δ22 (Table 1). The heterogeneity of rhBcl-2Δ22 in the absence of glycerol is also reflected by a high SOS (sum of squares) parameter, a measurement of the closeness of fit between the experimental data and an autocorrelation function, which expresses the relationship between the light scattering signal and the hydrodynamic radius of the molecule. In the presence of 0.5% (v/v) glycerol, the polydispersity number, and the SOS parameter, of rhBcl-2Δ22 were reduced to values representative of a nonaggregated monodisperse protein. The greater homogeneity of the protein in the presence of glycerol is consistent with the results of size exclusion chromatography. As a comparison, the hydrodynamic parameters for lysozyme and BSA are also included in Table 1.

Far-UV Circular Dichroism Spectrum of rhBcl2Δ22. rhBcl-2Δ22 exhibits no characteristic electronic absorption spectra other than the maximum absorption at 280 nm (data not shown). Analysis of the secondary structure composition

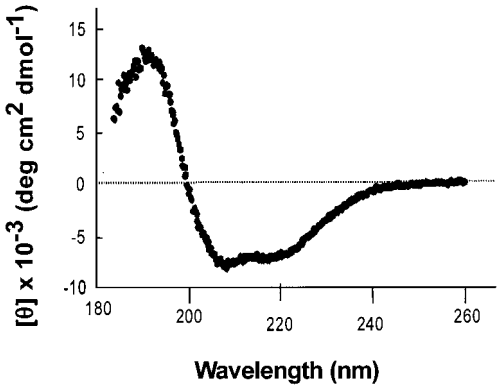

FIGURE 3: Far-UV CD spectrum of rhBcl-2Δ22 in 10 mM sodium phosphate (pH 8.0). The spectrum is the average of multiple scans corrected for the background.

of rhBcl-2Δ22 based on its primary sequence using the PHD method (*46*) predicts 44.9% α-helical, 6.7% *β*-sheet, and 48.4% random coil content. Consistent with this analysis, the far-UV CD spectrum of rhBcl-2Δ22 has absorption minima at 208 and 222 nm, which are characteristic of helical proteins (Figure 3). The overall CD spectrum of rhBcl-2Δ22 resembles that of Bcl-x_L (*47*), suggesting a similar secondary structure profile for rhBcl2-Δ22 and Bcl-x_L.

Stability of rhBcl-2Δ22. The thermodynamic stability of rhBcl-2Δ22 was analyzed by thermal denaturation. Unfolding and refolding of rhBcl-2Δ22 were monitored by the change in ellipticity at 222 nm as a function of temperature. Denaturation was only partially reversible under the conditions that were studied. The thermal unfolding curve shows a sharp transition suggesting a two-state mechanism, although other mechanisms are not excluded (Figure 4A). The melting temperature (T_m), determined from the midpoint of the thermal denaturation curve for rhBcl-2Δ22, was 62.8 °C. The susceptibility of rhBcl-2Δ22 to proteolytic degradation was also analyzed. Protein degradation was observed during incubation at room temperature, with a predominant 17 kDa fragment (Figure 4B). Complete degradation of rhBcl-2Δ22 was observed after incubation at room temperature for 4 days (Figure 4C, lane 1). This proteolytic cleavage was inhibited in the presence of EDTA or EGTA, suggesting rhBcl-2Δ22 is sensitive to calcium-dependent protease(s). A cocktail of common protease inhibitors (PMSF, aprotinin, pepstatin, and leupeptin) also protected rhBcl-2Δ22 from proteolysis (Figure 4D).

Pore Formation by rhBcl-2Δ22. Bcl-2 family proteins form pores in synthetic lipid vesicles (*17*, *48*, *49*). To study the pore-forming activity of rhBcl-2Δ22 protein, a fluorescent dye (ANTS) and its quencher (DPX) were encapsulated in large unilamellar vesicles (70:30 PC:PG) and release of the dye was monitored by the fluorescence of the suspension. Addition of rhBcl-2Δ22 induced fast and extensive release of ANTS from the liposomes, indicating that purified rhBcl-2Δ22 is active and correctly folded (Figure 5A). Pore formation occurred only at low pH, since no leakage was detected at pH >5.5. In addition, the presence of negatively charged lipids in the liposomes was required for efficient pore formation (Figure 5B). The identity of the negatively charged group on the phospholipid, however, did not have a significant effect on pore formation by rhBcl-2Δ22 (Figure 5C). Recombinant human Bcl-x_LΔ20 has similar requirements for pore formation in lipid membranes, although the specific pore-forming activity of Bcl-x_LΔ20 was significantly lower than that of Bcl-2Δ22 at all pH values that were tested (Figure 5D).

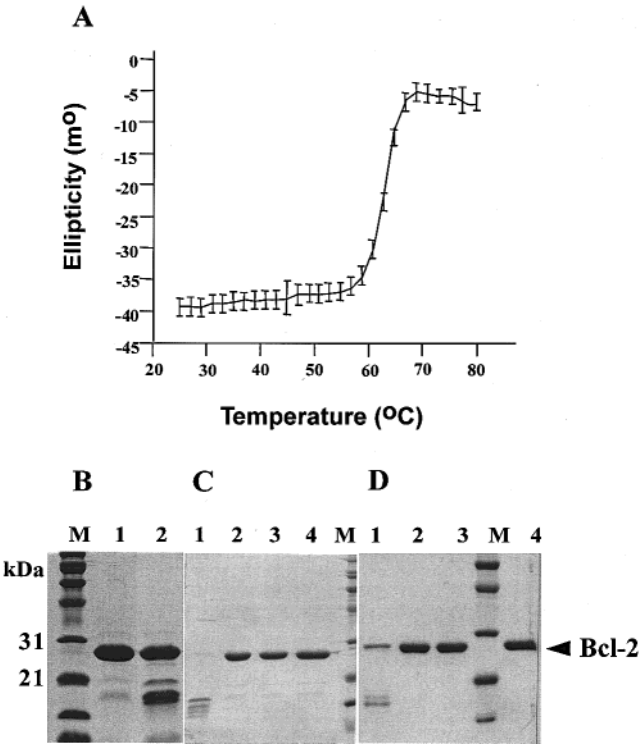

FIGURE 4: Stability of rhBcl-2Δ22. (A) Temperature dependence of the CD signal of rhBcl-2Δ22 at 222 nm. The protein concentration was 0.2 mg/mL in 10 mM sodium phosphate (pH 8.0). (B) Proteolysis of rhBcl-2Δ22 analyzed on 15% SDS−PAGE. An equal amount of purified rhBcl-2Δ22 was loaded on each lane after incubation at 4 °C (lane 1) and room temperature (lane 2) overnight. (C) rhBcl-2Δ22 (0.5 mg/mL) incubated at room temperature for 4 days before separation by SDS−PAGE. rhBcl-2Δ22 without metal chelator (lane 1), with 2 mM EDTA (lane 2), with 2 mM EGTA (lane 3), and with 2 mM EDTA and EGTA (lane 4). (D) rhBcl-2Δ22 incubated at room temperature in the absence of protease inhibitors and metal chelator (lane 1), in the presence of protease inhibitors, aprotinin, leupeptin, pepstatin A, and PMSF (lane 2), in the presence of excess protease inhibitors (lane 3), or in the presence of metal chelator, EGTA, and EDTA (lane 4). All lanes labeled M contained 200, 116, 97, 66, 45, 31, 21, 14, and 6 kDa marker proteins (from top to bottom); only the 31 and 21 kDa markers are indicated for clarity.

ANS Fluorescence Spectroscopic Studies Indicate Exposed Hydrophobic Regions on rhBcl-2Δ22. To test whether rhBcl-2Δ22 possesses an exposed hydrophobic region similar to that of Bcl-x_L (*7*, *8*), the binding of an extrinsic hydrophobic fluorescent probe, ANS, was examined by fluorescence spectroscopy. This probe fluoresces intensely when associated with hydrophobic regions on proteins such that the increase in fluorescence is an indicator of the relative hydrophobicity of a protein (*50*). Free ANS in solution has a relatively low fluorescence intensity with maximal emission at 516 nm (Figure 6A). In the presence of rhBcl-2Δ22, a strong increase in ANS fluorescence associated with a blue shift of the maximal emission wavelength (470 nm) is observed, indicative of ANS binding to rhBcl-2Δ22 (Figure 6A). Analysis by the continuous variation method (Job plot) demonstrated a maximal change in the fluorescence intensity for the ANS and rhBcl-2Δ22 complex at a molar stoichio-

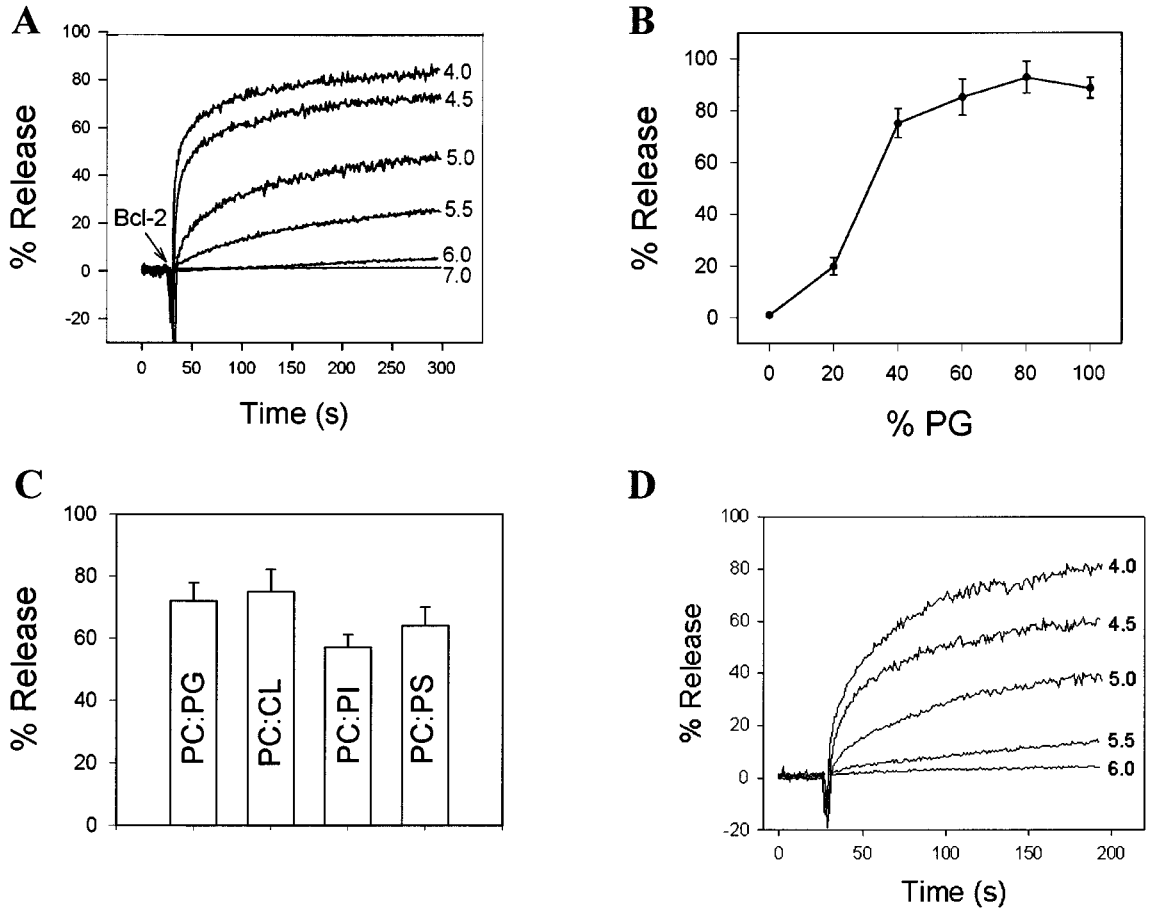

FIGURE 5: rhBcl-2Δ22 forms pores in large unilamellar vesicles. (A) Effect of pH on rhBcl-2Δ22-induced liposome leakage. The liposome composition was 70:30 PC:PG. Solutions were buffered with MES/KOH in the pH 6−7.0 range, and with potassium acetate/acetic acid in the pH 4−5.5 range. The arrow indicates the time of protein addition. (B) Effect of phosphatidylglycerol (PG) content on rhBcl-2Δ22-induced liposome leakage at pH 4.5. (C) Net negative electrical charge, but not a specific lipid moiety, is required for efficient pore formation. In all cases, liposomes contained 70% PC, and the pH was 4.5. (D) Effect of pH on Bcl-x_LΔ20-induced liposome leakage as described for panel A.

metric ratio of approximately 1:1, suggesting there is a specific, saturable binding site for ANS on rhBcl-2Δ22 (Figure 6B).

The BH3 peptide from Bak binds to the hydrophobic pocket formed by the BH1−3 domains of Bcl-x_L (*8*). To determine whether ANS also binds to the hydrophobic groove docking site for pro-apoptotic proteins, we examined whether a Bak BH3 16-residue peptide competed for a rhBcl-2Δ22 interaction using the ANS fluorescence assay. BH3 peptide did not affect ANS fluorescence in the absence of rhBcl-2Δ22 (data not shown). The change in ANS fluorescence intensity as a function of BH3 peptide concentration is shown in Figure 6C. A decrease in ANS fluorescence proportional to the added concentration of BH3 peptide was observed, indicating the displacement of bound ANS from rhBcl-2Δ22. In the presence of a molar excess of BH3 peptide, ANS fluorescence was not completely restored to that of free ANS in solution. This may be an indication of additional ANS binding sites on rhBcl-2Δ22 with lower binding affinity or the retention of a partial hydrophobic character at the hydrophobic groove occupied by the BH3 peptide. Incomplete reversal of the fluorescence enhancement on protein binding has also been reported for these fluorochromes (ANS and bis-ANS) with assays designed to assess the binding of small molecules, such as ATP or ADP, to hydrophobic sites on protein surfaces (*51*). Nevertheless, this study indicates that pro-apoptotic BH3 peptides and ANS compete for the same exposed hydrophobic binding site of Bcl-2. The binding site for ANS on rhBcl-2Δ22 is probably the hydrophobic cleft formed by the BH1−3 domains of rhBcl-2 as observed in Bcl-x_L (*8*).

Antimycin A Binds to the Hydrophobic Groove of rhBcl-2Δ22. We recently demonstrated that cells expressing high levels of Bcl-x_L are selectively killed by antimycin A (*34*). Unexpectedly, we also found that antimycin A can bind to the hydrophobic groove of Bcl-x_L. The potential interaction of antimycin A with rhBcl-2Δ22 was investigated using fluorescence spectroscopy. Unlike ANS, free antimycin A in solution has relatively high fluorescence. However, its fluorescence increases by as much as 30% in the presence of rhBcl-2Δ22, indicating a molecular interaction between antimycin A and rhBcl-2Δ22 (Figure 7A). The maximal change in fluorescence intensity of antimycin A with rhBcl-2Δ22 was observed at a molar stoichiometric ratio of approximately 1:1 (Figure 7B). The fluorescence enhancement of antimycin A with rhBcl-2Δ22 was reversed by addition of the Bak BH3 peptide (Figure 7A). This is due to displacement of bound antimycin A from rhBcl-2Δ22 and indicates that antimycin A binds to the hydrophobic groove of rhBcl-2Δ22.

We also assayed ligand binding to rhBcl-2Δ22 by isothermal calorimetry (Figure 7C). Thermodynamic data

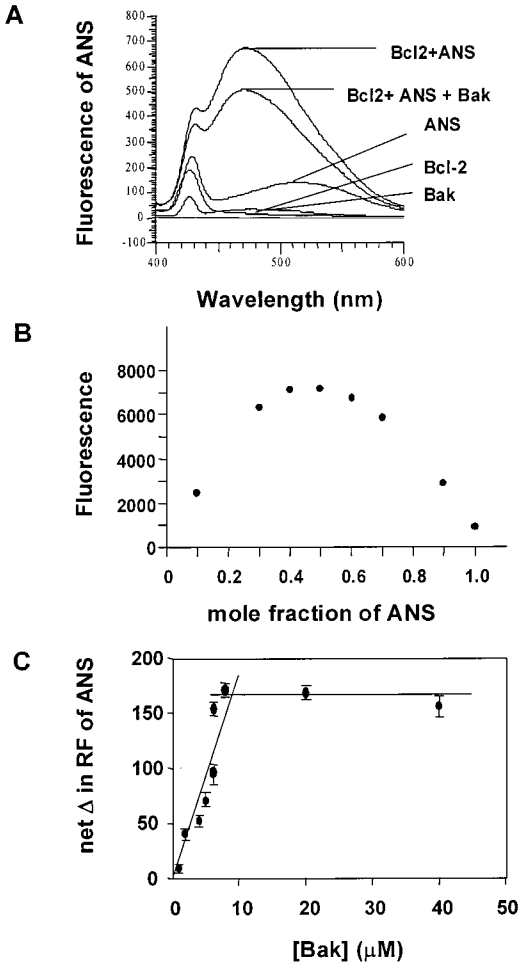

FIGURE 6: Binding of ANS to the rhBcl-2Δ22 protein is inhibited by the BH3 peptide. (A) Fluorescence emission spectra of the ANS−rhBcl-2Δ22 complex, ANS in the presence of rhBcl-2Δ22 and the BH3 peptide, ANS free in solution, rhBcl-2Δ22, and the BH3 peptide (from top to bottom). All concentrations were kept at 4 μM. (B) Job plot for binding of ANS to rhBcl-2Δ22. The enhanced relative fluorescence as a function of mole fraction of ANS is plotted. The sum of the concentrations of ANS and rhBcl-2Δ22 was held constant such that the total mole fraction is 1. (C) The net change (decrease) in relative fluorescence of ANS as a function of BH3 peptide concentration. The displacement of ANS from rhBcl-2Δ22 was determined by measuring the net decrease in fluorescence emission of ANS at various concentrations of added BH3 peptide after ANS was allowed to form a complex with rhBcl-2Δ22. Error bars represent standard deviations in fluorescence intensity from three independent experiments.

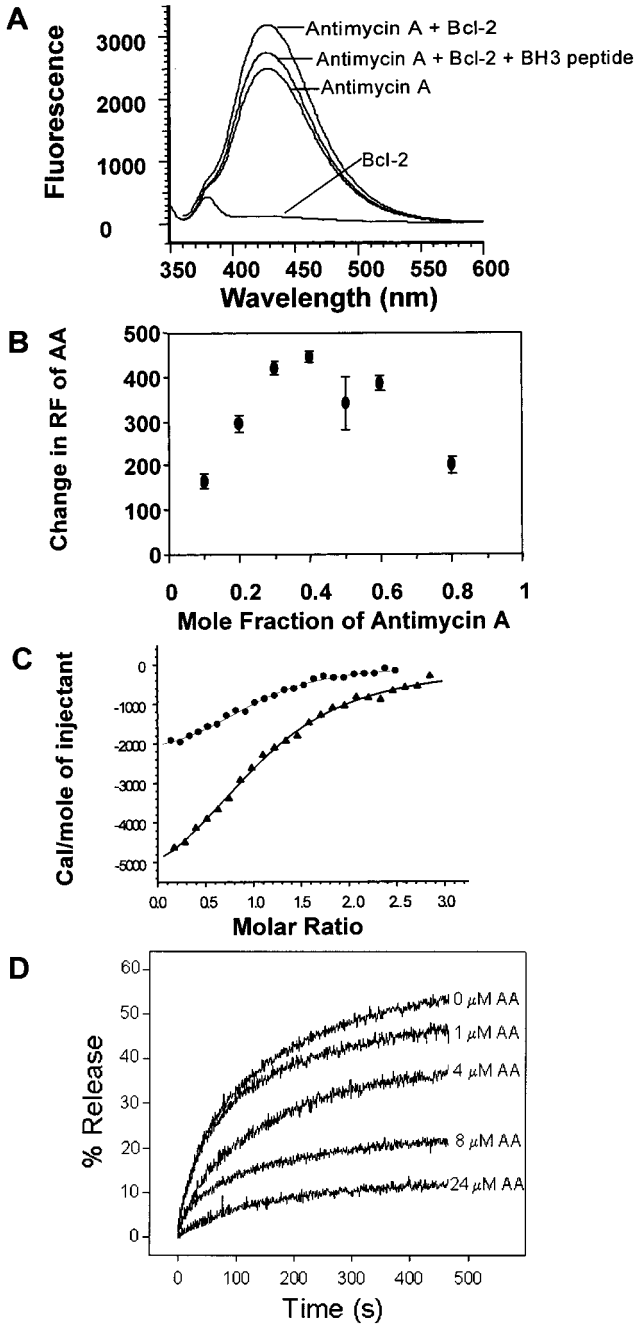

FIGURE 7: Antimycin A binds to rhBcl-2Δ22. (A) Relative fluorescence emission spectra of the antimycin A−rhBcl-2Δ22 complex, antimycin A (AA) in the presence of rhBcl-2Δ22 and the BH3 peptide, antimycin A free in solution, and the BH3 peptide (from top to bottom). Concentrations for AA, rhBcl-2Δ22, and the BH3 peptide were 3, 4.5, and 1.5 μM, respectively. The BH3 peptide did not affect antimycin A fluorescence in the absence of rhBcl-2Δ22. (B). Job plot for binding of AA to rhBcl-2Δ22. The net change in the enhanced relative fluorescence as a function of AA mole fraction is plotted. The sum of the concentrations of AA and rhBcl-2Δ22 was held constant at 5 μM. Error bars represent standard deviations in fluorescence intensity from three independent experiments. (C) Integrated heats from the calorimetric titrations of antimycin A_3 (▲) and the Bak BH3 peptide (●) binding to Bcl-2Δ22 at 298 K and their respective nonlinear least-squares fits (—). Raw data from 25 × 10 μL injections of 36 μM antimycin A_3 or 181 μM BH3 peptide into 1.3 mL of 2.2 or 13.2 μM Bcl-2Δ22, respectively, were corrected for heats of dilution prior to fitting to a model for single-site binding. (D) Inhibition of pore formation of Bcl-2 by antimycin A. Experiments were carried out as described in the legend of Figure 5 in the presence of the indicated concentration of antimycin A.

derived from these experiments are summarized in Table 2. The dissociation constant (K_d) for antimycin A_3 binding to rhBcl-2Δ22 is 0.82 μM, which is slightly lower than the value of 2.8 μM for BH3 binding. Both ligands show favorable enthalpic and entropic binding components, but it is difficult to directly compare the results for the two ligands since different solvent conditions were used. However, the relatively large entropy terms for each reaction indicate the ligand binding pocket is an exposed hydrophobic groove at the protein surface, since solvent release from such a groove, upon ligand binding, could provide a large, positive contribution to the total entropy change (*52*, *53*). In addition, the pore-forming activity of Bcl-2 was inhibited by antimycin A in an antimycin A concentration-dependent manner (Figure 7D).

Table 2: Experimental Thermodynamic Data for Antimycin A_3 and Bak BH3 Peptide Binding to Bcl-2Δ22 at 298 K

	antimycin A_3	Bak BH3
K_d (μM)	0.815 ± 0.072	2.85 ± 0.33
$\Delta H°$ (kcal/mol)	−6.54 ± 0.25	−2.45 ± 0.09
$\Delta S°$ (kcal mol^{-1} K^{-1})	5.91 ± 0.77	17.2 ± 0.9
$\Delta G°$ (kcal/mol)	−8.28 ± 0.73	−7.55 ± 0.88

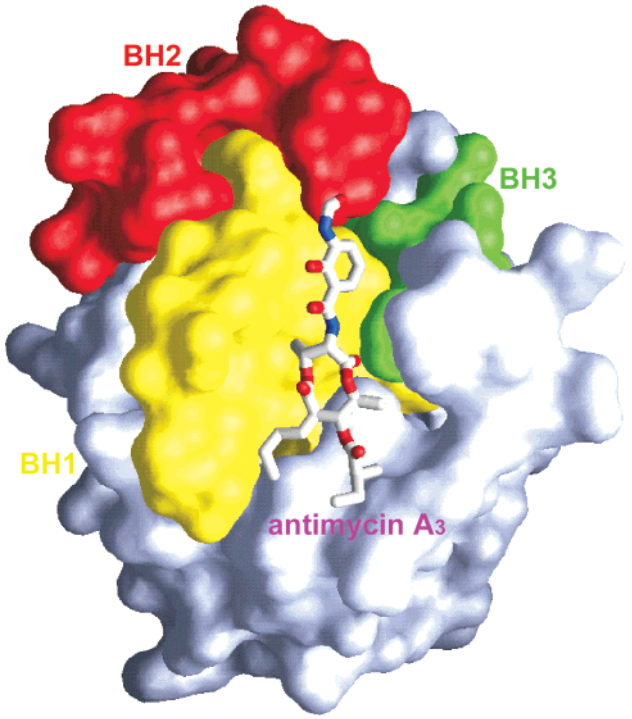

FIGURE 8: Molecular models of antimycin A_3 bound to hBcl-2Δ22. The hBcl-2Δ22 model structure is represented by a molecular surface diagram. The surface formed by residues from the conserved BH1−3 domains is color coded with yellow, red, and green, respectively. The rest of the surface is represented by light blue. The hydrophobic groove is formed by the residues from the BH1−3 domains. Antimycin A_3 is represented by a stick model, and the carbon, oxygen, and nitrogen atoms are colored gray, red, and blue, respectively. The top scoring orientation of antimycin A_3 binds hBcl-2Δ22 on the hydrophobic groove formed by the BH1−3 domains.

Molecular Modeling of hBcl-2Δ22 and the Predicted Binding Mode of Antimycin A3. Homology modeling of hBcl-2Δ22 using the software MODELLER demonstrates two central hydrophobic α-helices surrounded by five amphipathic helices. A hydrophobic groove at the protein surface is formed by the conserved BH1−3 regions similar to that in Bcl-x_L (*7*). The surface area of the predicted hydrophobic groove on hBcl-2Δ22 is slightly smaller than that found on the Bcl-x_L structure. Using a molecular docking program, DOCK, the antimycin A_3 molecule is predicted to bind at the same hydrophobic groove with the salicylate ring interacting with residues from the BH1−3 regions at the upper part of the groove, and the dilactone ring and aliphatic tail interacting with the BH1 region (Figure 8). The prediction of antimycin A binding to the hydrophobic groove of Bcl-2 by molecular modeling is consistent with the binding studies of antimycin A and Bcl-2.

Antimycin A Induces Apoptosis in Cell Lines Overexpressing hBcl-2. Since antimycin A binds to rhBcl-2Δ22 in addition to Bcl-x_L, we tested the apoptotic sensitivity of hBcl-2-expressing cells to this compound. Murine hepatocyte TAMH cells were stably transfected with pSFFV-hBcl-2 plasmids or control plasmids, and hBcl-2 protein expression was analyzed by Western blotting. Shown in Figure 9A is an immunoblot of expression of anti-apoptotic proteins hBcl-2 and Bcl-x_L in cell lysates from representative clonal cell lines. The clonal lines with high-level hBcl-2 expression (TAMH B3 and B5) were selected for further testing. In a side by side comparison, cells expressing hBcl-2 were as resistant to the chemotherapeutic drug, adriamycin, as their Bcl-x_L-transfected counterparts (Figure 9B). However, increased cell death of Bcl-2- or Bcl-x_L-overexpressing cells was observed upon antimycin A treatment compared to cells tranfected with vector alone. By light microscopy, the morphology of dying cells appeared to be apoptotic (Figure 9C). Additionally, activation of caspase-3 was detected within 2 h of antimycin A treatment of cells, which is consistent with apoptotic cell death (Figure 9D). However, hBcl-2-expressing cells required 5-fold higher concentrations of antimycin A than Bcl-x_L-expressing cells for comparable cytotoxicity to be observed (Figure 9B). This could be due either to the different expression levels of Bcl-2 and Bcl-x_L in the two cell lines or to the fact that the Bcl-2−antimycin A complex is less pro-apoptotic than the Bcl-x_L−antimycin A complex.

Despite the binding to the Bcl-2 hydrophobic groove, addition of the fluorochrome ANS did not trigger apoptosis of control or Bcl-2-expressing cells (Figure 9B). The inhibitory effect of antimycin A for Bcl-2 might, therefore, require a specific binding conformation. In addition, 2-methoxyantimycin A, an antimycin A analogue that is inactive for the inhibition of electron transfer in mitochondria (*54*, *55*), also selectively induced apoptosis in cells expressing Bcl-2 proteins (Figure 9B,C). Thus, the activity of antimycin A as an inhibitor of mitochondrial complex III is dispensable for its selective cytotoxicity against Bcl-2-expressing cells.

DISCUSSION

We describe a simple and rapid method for preparing the highly active human Bcl-2 protein from small-scale bacterial cultures. Expression of the rhBcl-2Δ22 protein with the transmembrane signal/anchor sequence removed resulted in 55 mg of homogeneous protein from a starting 6 L cell culture at the end of the final purification step. The yield of recombinant Bcl-2 protein from previously published methods is low and required either a macroscale fermentation, purification from inclusion bodies, or a combination of both for a larger quantity of protein to be obtained (~500 μg to >10 mg of Bcl-2) (*25*−*27*). The purified rhBcl-2Δ22 can be concentrated to >17 mg/mL in the absence of detergent, an ideal concentration for undertaking structural studies, compared to 0.5 mg/mL for mouse Bcl-2 (*26*).

Recombinant hBcl-2Δ22 gave a single protein band by SDS−PAGE after size exclusion chromatography, but IEF revealed two minor bands migrating at slightly lower pI than the major rhBcl-2Δ22 band at pI 6.8. This minor heterogeneity may arise from post-translational modification(s). Minor bands migrating close to the expected major protein band were observed for recombinant rat Bcl-x_L and mouse Bcl-2 (*26*, *56*), and attributed to post-translational deamidation of Asn to isoaspartate and aspartate (*56*). rhBcl2-Δ22 has a Asn-

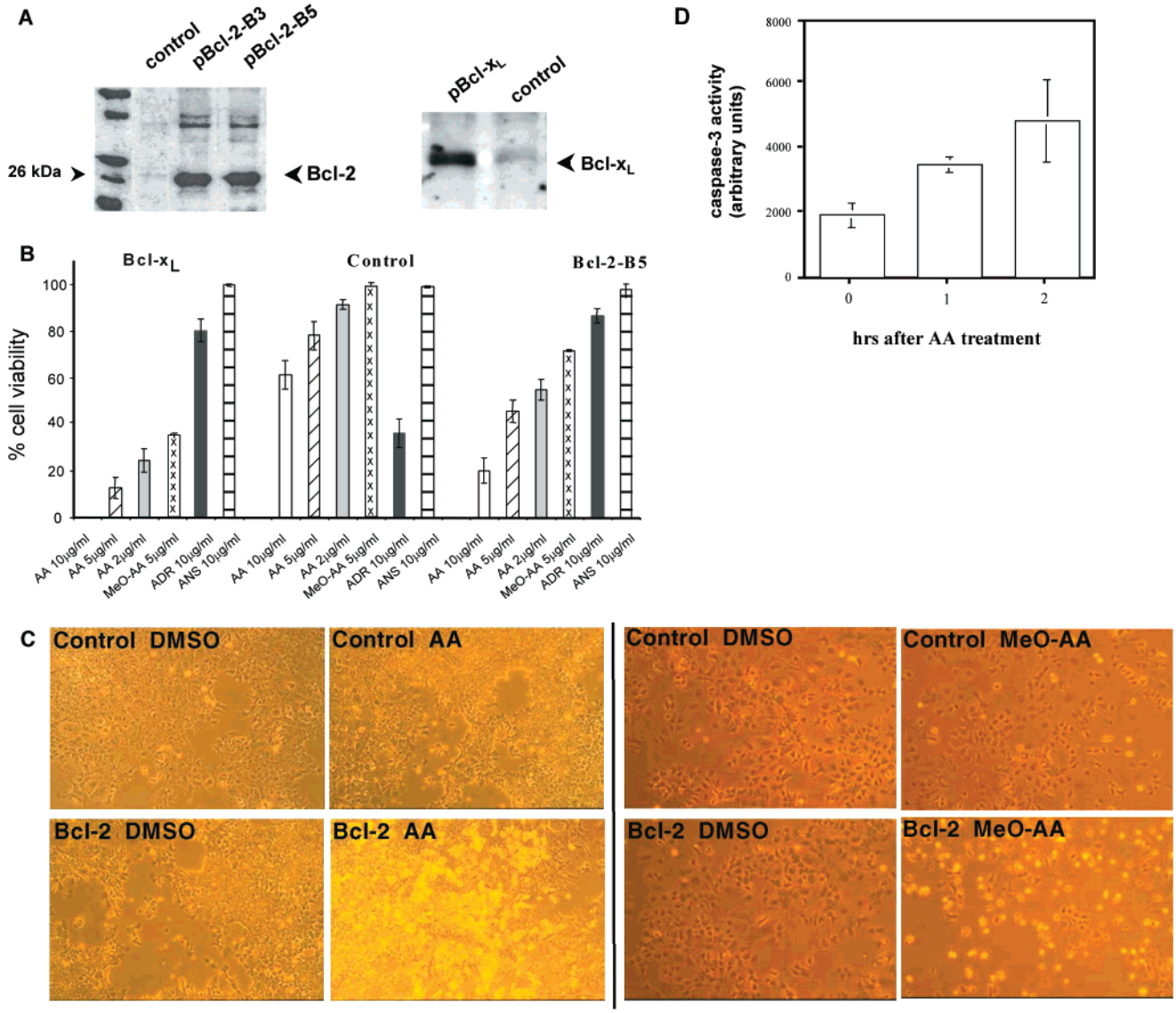

FIGURE 9: Antimycin A selectively induces apoptotic cell death in cell lines overexpressing Bcl-2 type proteins. (A) Western blot detection of hBcl-2 and Bcl-x_L expression in cells transfected with control, phBcl-2, or pBcl-x_L plasmids. pBcl-2-B3 and pBcl-2-B5 represent two independent clonal cell lines. The hamster anti-Bcl-2 monoclonal antibody and rabbit anti-Bcl-x_L antibody were used for the detection of Bcl-2 and Bcl-x_L, respectively. (B) Cells were treated with antimycin A_3 (AA), 2-methoxyantimycin A_3 (MeO-AA), and ANS for 6 h or adriamycin (ADR) for 24 h. Cell viability was determined by trypan blue staining. (C) Phase contrast microscopy of TAMH-neo (control) and Bcl-2 cells. Cells were treated with 5 μg/mL AA or MeO-AA in DMSO or vehicle alone for 4 h. (D) Activation of caspase-3 after antimycin A treatment. Cells were treated with 2 μg/mL AA, and 75 μg/mL cell lysate protein was incubated with 50 μM fluorogenic substrate, Ac-DEVD-AMC, in caspase assay buffer at 30 °C for 30 min. Fluorescence of assay solutions was measured at an excitation wavelength of 360 nm and an emission wavelength of 460 nm.

Gly sequence, which is susceptible to Asn deamidation and formation of isoaspartic acid and aspartate through a succinimide intermediate (*57*). Deamidation of Gln and oxidation of Met are other possibilities that would lower the net pI. The minor acidic protein band observed with a pI of 4.8 is probably a copurifying protein contaminant unrelated to Bcl-2. An anion exchange chromatographic step resolves these minor heterogeneities to yield the apparently homogeneous protein as shown in Figure 1.

Limited proteolysis studies of the murine Bcl-2 protein demonstrated the susceptibility to common protease, including the serine protease trypsin and cysteine protease papain (*26*). We also noticed the extreme susceptibility of rhBcl-2Δ22 to proteolysis during purification. Interestingly, EDTA or EGTA alone protected rhBcl-2Δ22 from proteolysis as effectively as several protease inhibitors, suggesting susceptibility of rhBcl-2Δ22 to metalloproteases, such as calcium-dependent proteases.

Previous studies suggested that Bcl-2 forms homodimers in yeast two-hybrid systems (*11*, *13*). Our studies by DLS, however, show that rhBcl-2Δ22 is monodisperse in nondenaturing solution, consistent with the recent observation (*58*). Similarly, mouse Bcl-2ΔTM and Bcl-x_L do not form homodimers (*26*, *59*). Conus et al. (*58*) recently demonstrated that Bcl-2 heterodimerizes but fails to homodimerize due to structural constraints of the conserved BH domains of Bcl-2. These observations suggest that the conserved BH1−3 domains are important for associations with, for example, Bax, implicating the regulatory mechanism for the Bcl-2 family through protein−protein interactions.

Secondary structure analysis based on the Bcl-2 primary sequence predicts that rhBcl-2Δ22 belongs to the class of

all α-helical proteins. This was confirmed by far-UV CD spectroscopy, which showed rhBcl-2Δ22 exhibiting the absorption minima characteristic of all α-helical proteins. By analogy with the X-ray structure of Bcl-x_L (*7*), the observed α-helices in rhBcl-2Δ22 likely include the conserved BH domains, as well as the regions whose sequences are highly identical with that of Bcl-x_L. The stability of rhBcl-2Δ22 analyzed by heat-induced denaturation is consistent with a two-state thermal unfolding process, normally observed for small globular proteins (*60*), with a T_m of 62.8 °C. A comparison with T_m values of unrelated proteins reveals that the thermostability of rhBcl-2Δ22 is comparable to that of the heat-stable metalloprotease of C-terminus thermolysin (*61*), thermophilic DNA binding protein *Bst*HU (*62*), 3-phosphoglycerate kinase (*63*), and equine milk lysozyme (*64*), and significantly more stable than other mesophilic proteins (*63*) and collagen (*65*). Unfortunately, T_m values are not available for other Bcl-2 family proteins for examining any correlations with other properties of these proteins. It would be of interest to examine the relation between Bcl-2 stability and its function, for example, the effect on pore-forming activity of Bcl-2 family proteins.

Pore formation by Bcl-2Δ22 in the liposome assay requires negatively charged phospholipids, with no tracer release from vesicles made up completely of neutral phosphatidylcholine. Synthetic liposomes containing 30% phosphatidylglycerol, cardiolipin, phosphatidylinositol, or phosphatidylserine were each permissive for Bcl-2 pore formation. These results are congruent with published results (*17, 49*). The lipid composition of the mitochondrial outer membrane is approximately 55% PC and 25% PE with the acidic phospholipid, PI, as a minor component (*66*). Intriguingly, the maximal level of pore formation by Bcl-2 was observed at pH <4.5. At this pH, the acidic phospholipid headgroups are highly protonated (*67*). It is apparent that the in vivo environment at the mitochondrial surface corresponds poorly to the optimal in vitro conditions determined for Bcl-2 pore activity. We cannot differentiate between membrane insertion or lipid interactions as accounting for the observed dependence of Bcl-2 pore function on negatively charged phospholipids.

Our molecular modeling studies suggested that hBcl-2 possesses a hydrophobic groove similar to that of Bcl-x_L, formed by the highly conserved BH1−3 domains. Simulated docking algorithms with the hBcl-2 model structure further predicted that a mitochondria complex III inhibitor, antimycin A, and the pro-apoptotic Bak BH3 peptide had spatially overlapping binding sites in the hydrophobic groove. Consistent with this analysis, we demonstrated by fluorescence spectroscopy that antimycin A binding to rhBcl-2Δ22 was stoichiometric and competed efficiently by the Bak BH3 peptide.

Small molecules that specifically target the hydrophobic grooves of Bcl-2 type proteins could mimic pro-apoptotic BH3 peptides and represent a novel, rational approach for antineoplastic therapy, particularly with tumor cells resistant to conventional chemotherapeutic drugs due to overexpression of Bcl-2-related proteins. We have determined that the mitochondrial inhibitor antimycin A binds directly to rhBcl-2Δ22 and selectively induces apoptosis in cell lines overexpressing hBcl-2. The affinity of binding of antimycin A to Bcl-2 (0.82 μM) is consistent with the amount of antimycin A (3.8−17 μM) used to trigger apoptosis in TAMH cells, and comparable to the affinity of binding of the pro-apoptotic Bak BH3 peptide to the protein (K_d = 2.8 μM). The nonspecific hydrophobic fluorochrome ANS did not have apoptotic activity, suggesting that specific binding conformations of small molecule ligand might be required for apoptotic activity. Antimycin A, as well as a 2-methoxy derivative that is not an inhibitor of mitochondrial respiration, mimics pro-apoptotic BH3 domain peptides in inhibiting the pore function of Bcl-2 (in this study) and Bcl-x_L (*34*). Antimycin A could serve as a template for the design of therapeutic agents that directly target Bcl-2 and selectively kill tumor cells that overexpress Bcl-2-related proteins. During the preparation of this paper, Wang et al. (*68*) also reported the discovery of a small nonpeptide ligand that binds to the Bcl-2 hydrophobic groove and has cytotoxicity for Bcl-2-expressing cells.

The knowledge of three-dimensional structures of Bcl-2 in complex with small molecule ligands will be critical for the design of Bcl-2 inhibitors, as well as building our understanding of the essential functions of this important class of proteins. The protein expression and purification methodology described herein should facilitate these studies.

ACKNOWLEDGMENT

We thank Dr. David Baker for access to the CD spectrometer at the University of Washington (Seattle, WA), Dr. Eugene C. Yi for his technical assistance with mass spectroscopy at the Institute for Systems Biology, Dr. Julian Simon for the gift of 2-methoxyantimycin A at Fred Hutchinson Cancer Research Center (FHCRC), and FHCRC biotechnology resource center staff for their technical assistance.

REFERENCES

1. Vaux, D. L., and Korsmeyer, S. J. (1999) *Cell 96*, 245−254.
2. Thompson, C. B. (1995) *Science 267*, 1456−1462.
3. Strasser, A., Hunag, D. C. S., and Vaux, D. L. (1997) *Biochim. Biophys. Acta 1333*, F151−F178.
4. Reed, J. C. (1995) *Curr. Opin. Oncol. 7*, 541−546.
5. Cleary, M. L., Smith, S. D., and Sklar, J. (1986) *Cell 47*, 19−28.
6. Farrow, S. N., and Brown, R. (1996) *Curr. Opin. Genet. Dev. 6*, 45−49.
7. Muchmore, S. W., Sattler, M., Liang, H., Meadows, R. P., Harlan, J. E., Yoon, H. S., Nettesheim, D., Chang, B. S., Thompson, C. B., Wong, S.-L., Ng, S.-C., and Fesik, S. W. (1996) *Nature 381*, 335−341.
8. Sattler, M., Liang, H., Nettesheim, D., Meadows, R. P., Harlan, J. E., Eberstadt, M., Yoon, H. S., Shuker, S. B., Chang, B. S., Minn, A. J., Thompson, C. B., and Fesik, S. W. (1997) *Science 275*, 983−986.
9. Suzuki, M., Youle, R. J., and Tjandra, N. (2000) *Cell 103*, 645−654.
10. Hunter, J. J., Bond, B. L., and Parslow, T. G. (1996) *Mol. Cell. Biol. 16*, 877−883.
11. Yin, X. M., Oltvai, Z. N., and Korsmeyer, S. J. (1994) *Nature 369*, 321−323.
12. Hanada, M., Aime-Sempe, C., Sato, T., and Reed, J. C. (1995) *J. Biol. Chem. 270*, 11962−11969.
13. Sato, T., Hanada, M., Bodrug, S., Irie, S., Iwama, N., Boise, L. H., Thompson, C. B., Golemis, E., Fong, L., Wang, H. G., et al. (1994) *Proc. Natl. Acad. Sci. U.S.A. 91*, 9238−9242.
14. Borner, C., Olivier, R., Martinou, I., Mattmann, C., Tschopp, J., and Martinou, J. C. (1994) *Biochem. Cell. Biol. 72*, 463−469.
15. Lee, J. H., Takahashi, T., Yasuhara, N., Inazawa, J., Kamada, S., and Tsujimoto, Y. (1999) *Oncogene 18*, 6183−6190.

16. Schlesinger, P. H., Gross, A., Yin, X. M., Yamamoto, K., Saito, M., Waksman, G., and Korsmeyer, S. J. (1997) *Proc. Natl. Acad. Sci. U.S.A. 94*, 11357−11362.
17. Minn, A. J., Velez, P., Schendel, S. L., Liang, H., Muchmore, S. W., Fesik, S. W., Fill, M., and Thompson, C. B. (1997) *Nature 385*, 353−357.
18. Schendel, S. L., Xie, Z., Montal, M. O., Matsuyama, S., Montal, M., and Reed, J. C. (1997) *Proc. Natl. Acad. Sci. U.S.A. 94*, 5113−5118.
19. Chou, J. J., Li, H., Salvesen, G. S., Yuan, J., and Wagner, G. (1999) *Cell 96*, 615−624.
20. McDonnell, J. M., Fushman, D., Milliman, C. L., Korsmeyer, S. J., and Cowburn, D. (1999) *Cell 96*, 625−634.
21. Zamzami, N., Marchetti, P., Castedo, M., Zanin, C., Vayssiere, J. L., Petit, P. X., and Kroemer, G. (1995) *J. Exp. Med. 181*, 1661−1672.
22. Green, D. R., and Reed, J. C. (1998) *Science 281*, 1309−1312.
23. Vander Heiden, M. G., Chandel, N. S., Williamson, E. K., Schumacker, P. T., and Thompson, C. B. (1997) *Cell 91*, 627−637.
24. Matsuyama, S., Llopis, J., Deveraux, Q. L., Tsien, R. Y., and Reed, J. C. (2000) *Nat. Cell Biol. 2*, 318−325.
25. Haldar, S., Jena, N., DuBois, G. C., Takayama, S., Reed, J. C., Fu, S. S., and Croce, C. M. (1994) *Arch. Biochem. Biophys. 315*, 483−488.
26. Vance, B. A., Zacharchuk, C. M., and Segal, D. M. (1996) *J. Biol. Chem. 271*, 30811−30815.
27. Anderson, M., Blowers, D., Hewitt, N., Hedge, P., Breeze, A., Hampton, I., and Taylor, I. (1999) *Protein Expression Purif. 15*, 162−170.
28. Hockenbery, D. M., Oltvai, Z. N., Yin, X. M., Milliman, C. L., and Korsmeyer, S. J. (1993) *Cell 75*, 241−251.
29. Mach, H., Middaugh, C. R., and Lewis, R. V. (1992) *Anal. Biochem. 200*, 74−80.
30. Laemmli, U. K. (1970) *Nature 227*, 680−685.
31. Mayer, L. D., Hope, M. J., and Cullis, P. R. (1986) *Biochim. Biophys. Acta 858*, 161−168.
32. Stewart, P. R. (1980) *Anal. Biochem. 104*, 10−14.
33. Hockenbery, D., Nunez, G., Milliman, C., Schreiber, R. D., and Korsmeyer, S. J. (1990) *Nature 348*, 334−336.
34. Tzung, S.-P., Kim, K. M., Basanex, G., Zimmerberg, J., Zhang, K. Y.-J., and Hockenbery, D. M. (2001) *Nat. Cell Biol. 3*, 183−191.
35. Cantor, C. R., and Schimmel, P. R. (1990) in *Biophyscial Chemistry*, pp 1135−1139, Freeman & Co., New York.
36. Wiseman, T., Williston, S., Brandts, J. F., and Lin, L. N. (1989) *Anal. Biochem. 179*, 131−137.
37. Thompson, J. D., Higgins, D. G., and Gibson, T. J. (1994) *Nucleic Acids Res. 22*, 4673−4680.
38. Sali, A., and Blundell, T. L. (1993) *J. Mol. Biol. 234*, 779−815.
39. Laskowski, R. A., MacArthur, M. W., Moss, D. S., and Thornton, J. M. (1993) *J. Appl. Crystallogr. 26*, 283−291.
40. Luthy, R., Bowie, J. U., and Eisenberg, D. (1992) *Nature 356*, 83−85.
41. Colovos, C., and Yeates, T. O. (1993) *Protein Sci. 2*, 1511−1519.
42. Kim, H., Esser, L., Hossain, M. B., Xia, D., Yu, C.-A., Rizo, H., Van der Helm, D., and Deisenhofer, J. (1999) *J. Am. Chem. Soc. 121*, 4902−4903.
43. Kuntz, I. D. (1992) *Science 257*, 1078−1082.
44. Kane, J. F. (1995) *Curr. Opin. Biotechnol. 6*, 494−500.
45. Hu, X., Shi, Q., Yang, T., and Jackowski, G. (1996) *Protein Expression Purif. 7*, 289−293.
46. Rost, B., and Sander, C. (1994) *Proteins 19*, 55−72.
47. Xie, Z., Schendel, S., Matsuyama, S., and Reed, J. C. (1998) *Biochemistry 37*, 6410−6418.
48. Reed, J. C. (1997) *Nature 387*, 773−776.
49. Schendel, S. L., Montal, M., and Reed, J. C. (1998) *Cell Death Differ. 5*, 372−380.
50. Rosen, C. G., and Weber, G. (1969) *Biochemistry 8*, 3915−3920.
51. Wiksell, E., and Larsson-Raznikiewicz, M. (1982) *J. Biol. Chem. 257*, 12672−12677.
52. Hilser, V. J., Gomez, J., and Freire, E. (1996) *Proteins 26*, 123−133.
53. Cooper, A. (1999) *Curr. Opin. Chem. Biol. 3*, 557−563.
54. Tokutake, N., Miyoshi, H., Satoh, T., Hatano, T., and Iwamura, H. (1994) *Biochim. Biophys. Acta 1185*, 271−278.
55. Miyoshi, H., Tokutake, N., Imaeda, Y., Akagi, T., and Iwamura, H. (1995) *Biochim. Biophys. Acta 1229*, 149−154.
56. Aritomi, M., Kunishima, N., Inohara, N., Ishibashi, Y., Ohta, S., and Morikawa, K. (1997) *J. Biol. Chem. 272*, 27886−27892.
57. Stephenson, R. C., and Clarke, S. (1989) *J. Biol. Chem. 264*, 6164−6170.
58. Conus, S., Kaufmann, T., Fellay, I., Otter, I., Rosse, T., and Borner, C. (2000) *EMBO J. 19*, 1534−1544.
59. Sedlak, T. W., Oltvai, Z. N., Yang, E., Wang, K., Boise, L. H., Thompson, C. B., and Korsmeyer, S. J. (1995) *Proc. Natl. Acad. Sci. U.S.A. 92*, 7834−7838.
60. Conejero-Lara, F., De Filippis, V., Fontana, A., and Mateo, P. L. (1994) *FEBS Lett. 344*, 154−156.
61. De Filippis, V., De Antoni, F., Frigo, M., Polverino de Laureto, P., and Fontana, A. (1998) *Biochemistry 37*, 1686−1696.
62. Kawamura, S., Kakuta, Y., Tanaka, I., Hikichi, K., Kuhara, S., Yamasaki, N., and Kimura, M. (1996) *Biochemistry 35*, 1195−1200.
63. Kumar, S., Tsai, C. J., and Nussinov, R. (2000) *Protein Eng. 13*, 179−191.
64. Griko, Y. V., Freire, E., Privalov, G., van Dael, H., and Privalov, P. L. (1995) *J. Mol. Biol. 252*, 447−459.
65. Tomita, M., Ohkura, N., Ito, M., Kato, T., Royce, P. M., and Kitajima, T. (1995) *Biochem. J. 312*, 847−853.
66. Tzagoloff, A. (1982) *Cellular organelles*, Plenum Press, New York.
67. Tsui, F. C., Ojcius, D. M., and Hubbell, W. L. (1986) *Biophys. J. 49*, 459−468.
68. Wang, J. L., Liu, D., Zhang, Z. J., Shan, S., Han, X., Srinivasula, S. M., Croce, C. M., Alnemri, E. S., and Huang, Z. (2000) *Proc. Natl. Acad. Sci. U.S.A. 97*, 7124−7129.

BI002368E